Reprinted from JOURNAL OF SPACECRAFT AND ROCKETS, Vol. 15, No. 6, November–December, 1978, pp. 341–347

Dynamics of Short Eccentric Plain Seals with High Axial Reynolds Number

P. E. Allaire,* C. C. Lee,† and E. J. Gunter‡
University of Virginia, Charlottesville, Va.

Plain seals with high axial flow rates produce large stiffness and damping coefficients that can help stabilize high-speed rotating machinery. When the shaft is eccentric in the seal, a Bernoulli effect low-pressure region occurs on the large-clearance side of the shaft. A fluid-restoring force tends to center the shaft and reduce vibrations. This work extends the previous theory for short plain centered seals to large eccentricities using a perturbation analysis. Surface roughness effects are also included. An analysis of seals used in the Space Shuttle main engine hydrogen fuel turbopump indicates the desirability of plain seals over the labyrinth type. Experimental results confirm this.

Nomenclature

c = radial clearance, m
C_{ij} = damping coefficients, N-s/m
$\bar{C}_{ij}$ = $C_{ij}\,c/RL\Delta pt_c$, dimensionless damping
e = eccentricity
F = hydrostatic seal force, N
$\bar{F}$ = $F/RL\Delta p$, dimensionless force
h = film thickness, m
H = h/c, dimensionless film thickness
K_{ij} = stiffness coefficient, N/m
$\bar{K}_{ij}$ = $K_{ij}\,c/RL\Delta p$, dimensionless stiffness
L = length of seal, m
p = pressure, N/m^2
P = $p/\rho u_c{}^2$, dimensionless pressure
R = shaft radius, m
Re = axial Reynolds number, $2uh/\nu$
t, T = time, s, $T=t/t_c$
t_c = L/u_c, centered mean flow time
t_m, T_m = L/u, $T_m=t_m/t_c$, mean flow time
u = axial velocity, m/s
U = u/u_c, dimensionless axial velocity
u_c = centered axial velocity, m/s
W = applied, load, N
$\bar{W}$ = $W/RL\Delta p$, dimensionless load
x = horizontal coordinate, m
y = vertical coordinate, m
z, Z = axial coordinate, m, $Z=z/L$
δ = $\epsilon_r/2c$, relative roughness
λ = friction factor
ρ = specific weight, N/m^3
ξ = entrance loss coefficient
σ = $\lambda L/c$, seal friction coefficient
ν = kinematic viscosity, m^2/s
θ = angular coordinate system measured from positive x axis
ϵ = e/c, eccentricity ratio
ϵ_r = roughness, m
ψ = attitude angle

Subscripts

i = inlet
e = exit
0 = steady state (zeroth perturbation)
1 = first-order perturbation
c = centered case

Received Nov. 7, 1977; revision received June 5, 1978.

Index categories: Hydrodynamics; Nozzle and Channel Flow; LV/M Vibration.

*Associate Professor, Mechanical and Aerospace Engineering Department.
†Research Engineer, Mechanical and Aerospace Engineering Department.
‡Professor, Mechanical and Aerospace Engineering Department.

Introduction

THE fluid dynamics of flow in annular seals, shown in Fig. 1, can have dramatic effects on vibrations in rotating machinery.[1-9] Hydrodynamic forces generated in these seals can drive one machine unstable or contribute strongly to the stability of another machine. Usually seals with a relatively small axial Reynolds number, such as oil seals with a Reynolds number below 2000, are in the destabilizing category. Seals for liquids with low viscosity, such as water or liquid hydrogen, often have Reynolds number well above 2000. They tend to produce large seal stiffness and damping coefficients that can be beneficial to rotor stability.

Annular controlled leakage seals have been employed in the Space Shuttle main engine (SSME) high-pressure fuel turbopump (HPFTP) to improve stability. Large subsynchronous vibrations were encountered in tests of the SSME HPFTP with labyrinth seals and the original soft bearing supports. It was found that changing the seals to plain annular seals and making the bearing supports stiffer could possibly stabilize the rotor. Experimental results have verified the improvement in stability.

Liquid hydrogen at cryogenic temperatures is the working fluid in the HPFTP pump. Extremely low kinematic viscosity, approximately 3.5×10^{-7} m^2/s (2.26×10^{-4} in.^{2}/s), combines with high pressure drop across the seals, about 14 MPa (2030 lb$_f$/in.^{2}), to produce large axial flow rates. Axial Reynolds numbers in the range 100,000 to 500,000 result. The seal land length to shaft diameter ratio of about 0.16 produces circumferential fluid velocities that are small compared to axial fluid velocities. Calculated circumferential Reynolds numbers are approximately 1/5 of the axial Reynolds number.

Plain seals with large axial Reynolds number exhibit a "Bernoulli" type of effect when the shaft is eccentric in the seal. For a given axial pressure drop across the seal, the axial fluid velocity is larger in the large-clearance portion of the annulus than in the small-clearance region. Correspondingly, the pressure in the large-clearance side is lower than in the small-clearance portion, generating a hydrodynamic force in the direction opposite to the shaft eccentricity. It has been

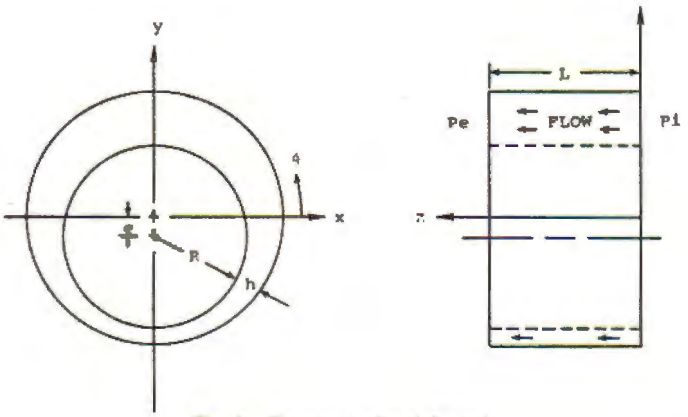

Fig. 1 Geometry of a plain seal.

shown both theoretically[3] and experimentally[4] that the force exists even if the shaft does not rotate. This restoring force effect leads to the calculation of dynamic coefficients for use in linear vibration analysis such as critical speeds, unbalance response, and stability.

A recent series of papers by Black et al.[3-9] has developed the theory for centered seals. The fluid equations of motion are based on a semiempirical bulk flow theory formally developed by Hirs.[10] Blasius-type friction factor formulas used in the theory are taken from experimental work by Yamada.[11-13]

This work extends the theory for short plain seals to large eccentricities and includes surface roughness effects. Shaft rotation effects are not considered in the analysis except as a change in axial pressure drop occurs with speed. The continuity and momentum equations are solved using a perturbation approach. An analysis of the SSME HPFTP is then used as an example to illustrate the application of the seal for rotating machinery stabilization.

Fluid Equations

The basic equations of motion for this flow have been derived by Hirs[10] using a bulk flow theory. Average bulk flow velocities both in the axial and circumferential flow directions are employed rather than law-of-the-wall, eddy-viscosity concepts, and time-averaged velocity profiles. The bulk flow theory is an extension of a Blasius-type turbulent pipe flow analysis and a turbulent Couette flow between rotating cylinders. Hirs' semiempirical theory is in excellent agreement with the law-of-the-wall theories at high Reynolds number and is suitable for extension to rough surfaces at very high axial Reynolds numbers.

Although the general equations of motion have been formulated in closed form, they have not been solved for an eccentric seal. This work considers a short eccentric seal without shaft rotation. A perturbation theory is used to obtain an analytical solution for the pressure in the seal. The seals in the HPFTP approximate this case because the length-to-diameter ratio is about 0.16, and the axial flow Reynolds number is usually an order of magnitude larger than the circumferential flow Reynolds number. One of the important effects that rotational HPFTP speed has on the seals is that the pressure drop across the seals increases dramatically with speed. Details are given in the example analysis.

The continuity and momentum equations[4] are

$$h\frac{\partial u}{\partial z}+\frac{\partial h}{\partial t}=0 \tag{1}$$

$$-\frac{1}{\rho}\frac{\partial p}{\partial z}=\lambda\frac{u^2}{h}+u\frac{\partial u}{\partial z} \tag{2}$$

where the local fluid acceleration term $\partial u/\partial t$ has been neglected (see Appendix A for justification). As flow in the circumferential direction is assumed small, the circumferential momentum equation is not considered. Circumferential pressure gradients exist because the shaft eccentricity creates circumferential gradients in the axial velocity and differing losses. The boundary conditions are[4]

$$p|_{z=0}=p_i-\tfrac{1}{2}(1+\xi)\rho u^2|_{z=0} \tag{3}$$

$$p|_{z=L}=p_e \tag{4}$$

where $\frac{1}{2}(1+\xi)\rho u^2|_{z=0}$ is the head loss.[4,16]

Equations (1) and (2) can be placed in dimensionless form as

$$H\frac{\partial U}{\partial Z}+\frac{\partial H}{\partial T}=0 \tag{5}$$

$$-\frac{\partial P}{\partial Z}=\frac{\sigma}{H}U^2+U\frac{\partial U}{\partial Z} \tag{6}$$

with the boundary conditions

$$P|_{Z=0}=P_i-\tfrac{1}{2}(1+\xi)U^2|_{Z=0} \tag{7}$$

$$P|_{Z=1}=P_e \tag{8}$$

The film thickness H is a function of θ, whereas both the velocity U and pressure P are functions of θ as well as Z.

The approach taken here is similar to the small-perturbation method developed by Black[4] but extended to include eccentric seals. Let the perturbation variables be

$$H=H_0+H_1 \qquad U=U_0+U_1 \qquad P=P_0+P_1$$

In each case, the subscript zero denotes the steady-state variables H_0, U_0, P_0 with the shaft at a fixed position in space, whereas the subscript 1 indicates either small displacements or small velocities about the fixed shaft position with the resulting change of fluid velocity U_1 and pressure P_1. This method yields linearized stiffness and damping coefficients that are used in the full rotor-bearing-seal model.

Retaining only zeroth-order terms yields the equations

$$H_0\frac{\partial U_0}{\partial Z}=0 \tag{9}$$

$$-\frac{\partial P_0}{\partial Z}=\frac{\sigma}{H_0}U_0^2 \tag{10}$$

with the boundary conditions

$$P_0|_{Z=0}=P_i-\tfrac{1}{2}(1+\xi)U_0^2|_{Z=0} \tag{11}$$

$$P_0|_{Z=1}=P_e \tag{12}$$

The first-order terms give the equations

$$H_0\frac{\partial U_1}{\partial Z}+\frac{\partial H_1}{\partial T}=0 \tag{13}$$

$$-\frac{\partial P_1}{\partial Z}=2\frac{\sigma}{H_0}U_0U_1-\frac{\sigma}{H_0^2}U_0^2H_1+U_0\frac{\partial U_1}{\partial Z} \tag{14}$$

with the boundary conditions

$$P_1|_{Z=0}=-(1+\xi)U_0U_1|_{Z=0} \tag{15}$$

$$P_1|_{Z=1}=0 \tag{16}$$

All terms with two first-order variables multiplied together have been neglected.

For the zeroth-order equations, the solution that satisfies the exit boundary condition at $Z=1$ is

$$P_0 = P_e + (\sigma/H_0)(1-Z)U_0^2 \tag{17}$$

At the inlet end, the pressure must satisfy the inlet boundary condition, which yields

$$\Delta P = P_i - P_e = \tfrac{1}{2}(1+\xi+2\sigma/H_0)U_0^2 \tag{18}$$

Normally the pressure drop ΔP is known rather than the fluid velocity U_0. However, the fluid velocity is contained within the expression for σ, and so Eq. (18) cannot be solved explicitly for U_0. An iterative procedure must be used.

The first-order pressure equation is

$$\frac{\partial^2 P_1}{\partial Z^2} = \frac{2\sigma}{H_0^2} U_0 \frac{\partial H_1}{\partial T}$$

which is obtained by elminating U_1 from Eqs. (13) and (14). The corresponding boundary conditions are

$$\left[\frac{2\sigma}{H_0} P_1 - (1+\xi)\frac{\partial P_1}{\partial Z}\right]\Big|_{Z=0}$$

$$= -(1+\xi)\left[\frac{\sigma}{H_0^2} U_0^2 H_1 + \frac{U_0}{H_0}\frac{\partial H_1}{\partial T}\right] P_1\Big|_{Z=0} = 0$$

Solving yields

$$P_1 = \frac{\sigma}{H_0^2} U_0 \frac{\partial H_1}{\partial T}(Z^2 - Z) + \frac{1+\xi}{1+\xi+2\sigma/H_0}\left[\frac{\sigma}{H_0^2} U_0^2 H_1 + \left(1+\frac{\sigma}{H_0}\right)\frac{U_0}{H_0}\frac{\partial H_1}{\partial T}\right](Z-1) \tag{19}$$

This completes the solution of the pressure perturbation equations.

Load Capacity

The steady-state load capacity of the seal is obtained by integrating the zeroth-order pressure P_0 over the entire seal surface:

$$\begin{Bmatrix} \bar{F}_x \\ \bar{F}_y \end{Bmatrix} = -\int_0^{2\pi}\left[\int_0^1 P_0 dz\right]\begin{Bmatrix}\cos\theta \\ \sin\theta\end{Bmatrix} d\theta$$

Employing the pressure from Eq. (17), the integration in the axial direction can be easily carried out analytically, since U_0 is not a function of Z.

The final result is

$$\begin{Bmatrix} \bar{F}_x \\ \bar{F}_y \end{Bmatrix} = -\int_0^{2\pi} \frac{\sigma/H_0}{1+\xi+2\sigma/H_0}\begin{Bmatrix}\cos\theta \\ \sin\theta\end{Bmatrix} d\theta \tag{20}$$

where the circumferential integral must be evaluated numerically, as both σ and H_0 are functions of θ. Clearly, for a centered seal, both σ and H_0 are constants, and so the load capacity is zero.

It is assumed for convenience that the applied load W is vertically downward. The steady-state equilibrium conditions require that $F_x = 0$ and $F_y = W$, or, in dimensionless terms,

$$\bar{F}_x = 0 \qquad \bar{F}_y = \bar{W}$$

As seen from Eqs. (17) and (18), P_0 and U_0 are symmetric about the y axis, indicating that the equilibrium position of the shaft must be along the negative y axis. If the dimensionless shaft eccentricity is ϵ, then the shaft position is $X=0$, $Y=-\epsilon$.

Figure 2 shows the dimensionless load capacity $\bar{W}$ vs the seal friction coefficient σ_c for a centered seal with various values of shaft eccentricity. Values for $Re>4000$ and $\epsilon_r=0.0$ were chosen so that the flow is above the transition range even near the wall for $\epsilon=0.90$ but well below the range where surface roughness becomes important. The results are plotted here as a function of the friction coefficient in the manner of Black[4,7] because $\bar{W}$ is a function only of σ_c, ϵ, and ξ, as seen from Eq. (20). Relations among σ_c and the axial Reynolds number, L/c, the pressure drop, surface roughness, etc., are given in Eq. (18) and Appendix B.

It can be seen that the load capacity curves all peak for some value of friction coefficient. This can be explained in the following manner. At high values of σ_c (corresponding to low Re), the pressure differences in the seal for a given eccentricity are small. Equation (20) shows that σ_c is large compared to $1+\xi$, and so the pressure drop is due almost solely to friction loss and is linear all around the seal. As the friction coefficient drops (corresponding to higher ΔP and Re), the Bernoulli effect becomes stronger, and the load capacity increases. Very small values of friction coefficient (corresponding to very large pressure drops and axial Reynolds number) induce such large head losses that the friction loss is very small, and the pressure tends toward a constant value around and along the shaft. Note that the numerator in Eq. (20) becomes small

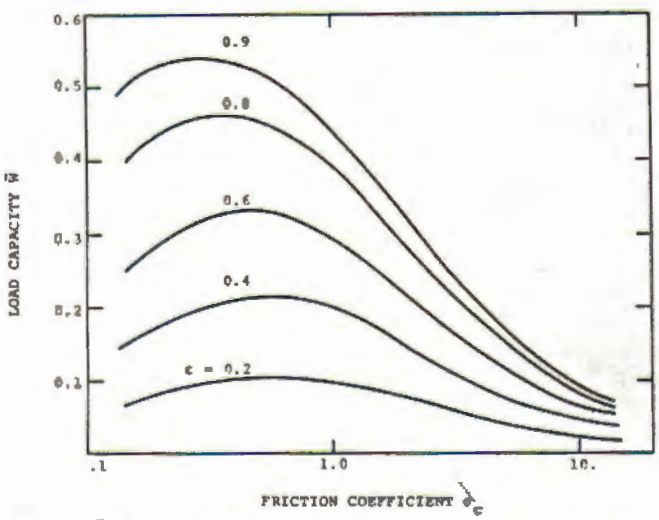

Fig. 2 Load capacity vs friction at different eccentricity ratios for a smooth seal ($Re>4000$).

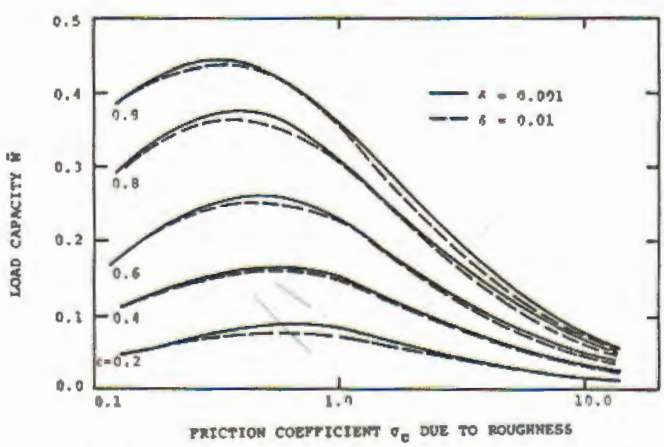

Fig. 3 Load capacity vs friction at different eccentricity ratios when roughness is encountered.

compared to the denominator when the friction coefficient becomes small.

Figure 3 shows the effects of relative surface roughness $\delta = \epsilon_r/2c$ on the load capacity. Only a small difference exists between the curves for the two values $\delta = 0.001$ and $\delta = 0.01$. However, for a given pressure drop in seals with two different surface roughnesses, a much different value of σ_c and resulting $\bar{W}$ will occur.

Stiffness and Damping Coefficients

The dynamic coefficients (similar to those for a plain journal bearing) are obtained by taking orthogonal perturbations of displacement or velocity about the equilibrium position. Integrating Eq. (19) and taking displacement perturbations in both the x and y directions yields

$$\begin{Bmatrix} \bar{K}_{xx} \\ \bar{K}_{yx} \end{Bmatrix} = \int_0^{2\pi} \left[\frac{1}{\sigma} \mu_0 \cos\theta \right] \begin{Bmatrix} \cos\theta \\ \sin\theta \end{Bmatrix} d\theta \tag{21}$$

$$\begin{Bmatrix} \bar{K}_{xy} \\ \bar{K}_{yy} \end{Bmatrix} = \int_0^{2\pi} \left[\frac{1}{\sigma} \mu_0 \sin\theta \right] \begin{Bmatrix} \cos\theta \\ \sin\theta \end{Bmatrix} d\theta \tag{22}$$

Taking the velocity perturbations gives

$$\begin{Bmatrix} \bar{C}_{xx} \\ \bar{C}_{yx} \end{Bmatrix} = \int_0^{2\pi} \frac{1}{\sigma} \mu_1 T_m \cos\theta \begin{Bmatrix} \cos\theta \\ \sin\theta \end{Bmatrix} d\theta \tag{23}$$

$$\begin{Bmatrix} \bar{C}_{xy} \\ \bar{C}_{yy} \end{Bmatrix} = \int_0^{2\pi} \frac{1}{\sigma} \mu_1 T_m \sin\theta \begin{Bmatrix} \cos\theta \\ \sin\theta \end{Bmatrix} d\theta \tag{24}$$

In each of these expressions, the integration with respect to Z from 0 to 1 has been carried out, but the circumferential integration must be evaluated numerically. The terms μ_0 and μ_1 are defined as

$$\mu_0 = \frac{1 + \xi + (\sigma^2/H_0^2)}{D_0} \tag{25}$$

$$\mu_1 = \left[(1+\xi) \frac{\sigma}{H_0} + \frac{4}{3} (1+\xi) \frac{\sigma^2}{H_0^2} + \frac{2}{3} \frac{\sigma^3}{H_0^3} \right] \times D_0^{-3/2} \tag{26}$$

where

$$D_0 = (1 + \xi + 2\sigma/H_0)^2 \tag{27}$$

These two quantities reduce to the same coefficients derived by Black[4] when σ is replaced by σ_c (centered value).

The dynamic coefficients of a plain seal with turbulent axial flow above Reynolds number of 4000 are shown in Figs. 4-7 for various values of shaft eccentricity. It can easily be seen that the stiffness is nearly independent of eccentricity for high seal friction coefficient σ_c (corresponding to a Reynolds number range approximately 4000-10,000). This is in agreement with the load capacity curves in Fig. 2 which are equally spaced, indicating that the derivative of W with respect to ϵ is nearly constant. At low values of σ_c, the effects of surface roughness begin to take over (see Appendix C).

Space Shuttle Application

Liquid hydrogen at cryogenic temperature is the working fluid in the hydrogen pump. Two plain seals, shown in Fig. 8, each consist of three lands of length, $L = 12.7$ mm (0.50 in.). The shaft diameter is $D = 79.8$ mm (3.14 in.) where there is very small step change in the diameter of the seal, but the clearance c is constant at 0.14 mm (0.0055 in.). The pressure drop across the seal is 14 MPa (2060 psi) when the pump is operating at full power level (37,400 rpm). The density and kinematic viscosity of the hydrogen are 3.30×10^{-4} kg/cm^3 (7.64×10^{-5} slugs/in.^{3}) and 1.55×10^{-7} m^2/s (2.41×10^{-4} in.^{2}/s), respectively.

A comparison of the axial Reynolds number with the circumferential Reynolds number shows that the axial value is larger by an order of magnitude at all speeds. This is due to the increase in ΔP with speed. The larger axial Reynolds number implies that the assumption of zero circumferential flow is reasonable.

No direct information is available, experimentally or analytically, to determine the static load on the SSME HP-FTP seal. Steady-state radial hydrodynamic loads occur on the pump turbine and compressor wheels, as well as inlet and outlet ducts. Small misalignments between the two bearing and seal centers also contribute to radial loads. Indirect evidence, from the rapid rate at which the ball bearings have worn, indicates that static radial loads may be large and the eccentricities above $\epsilon = 0.5$.

Stiffness and damping coefficients are calculated for each land and multiplied by three for the full seal results. Figures 9 and 10 show the seal coefficients vs eccentricity for both a smooth seal, $\epsilon_r = 0$, and a rough seal with an estimated roughness $\epsilon_r = 0.51$ μm (20 μin.) or relative roughness

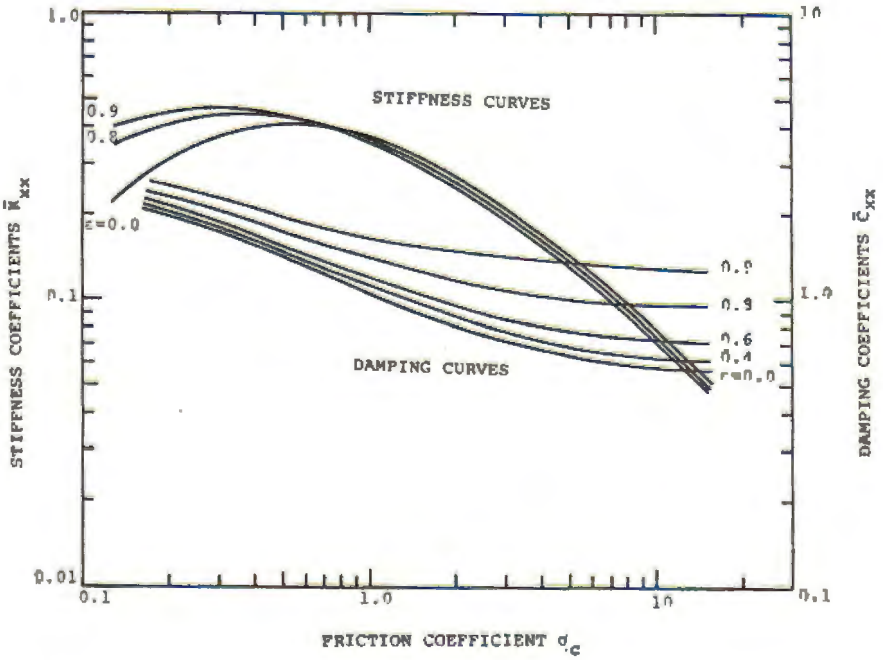

Fig. 4 Stiffness $\bar{K}_{xx}$ and damping $\bar{C}_{xx}$ vs friction at different eccentricity ratios.

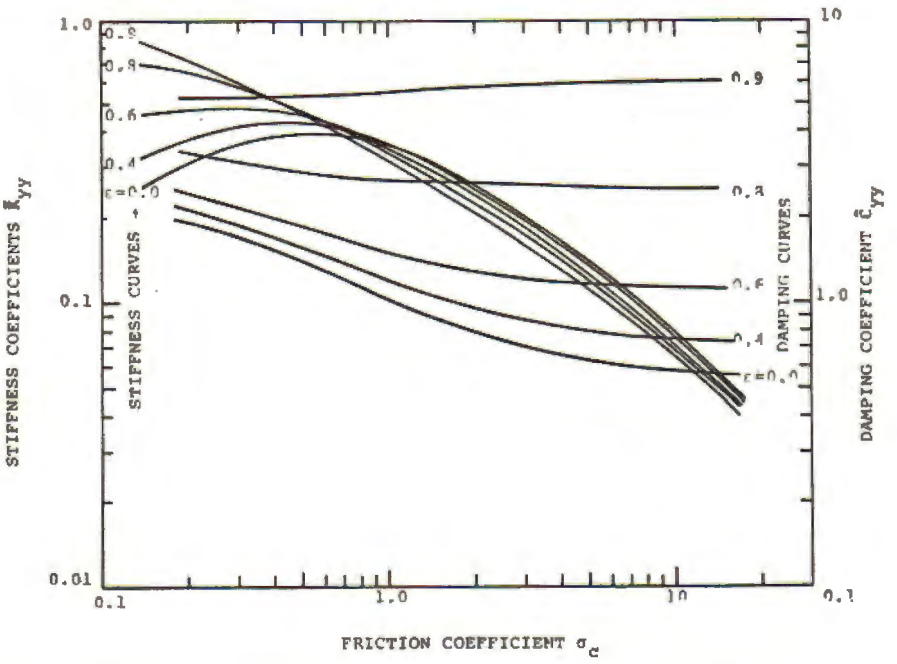

Fig. 5 Stiffness $\bar{K}_{yy}$ and damping $\bar{C}_{yy}$ vs friction at different eccentricity ratios.

$\delta = 0.00046$. The plots indicate that the stiffness is not a strong function of eccentricity, varying by about a factor of 2 over the range of eccentricity. For the damping, the variation is more like a factor of 3.

The point of major importance indicated by these plots is that the stiffness coefficients are of the same order of magnitude as the bearing-support structure. Bearing-support stiffness is estimated at 4.83×10^9 N/m (700,000 lb/in.) for each support located at the shaft ends, whereas the two compressor interstage seals have stiffness approximately 2.41×10^9 N/m (350,000 lb/in.) located near the rotor center. Thus, the seals can contribute a strong stiffening effect to the rotor, raising the critical speeds and rotor stability.

Another effect of importance is the damping delivered by the seals. By a conservative extimate, the damping coefficient for each seal is approximately 7015.03 N-s/m (40 lb-s/in.) near the center of the shaft. The damping at the bearing-support location is expected to be very low because the ball-bearings with a small deadband clearance (to allow for axial thermal growth) have no mechanisms to provide much damping. A value of 876.88 N-s/m (5 lb-s/in.) is considered the probable value. This indicates that the seals may provide much larger damping than any other mechanism in the pump.

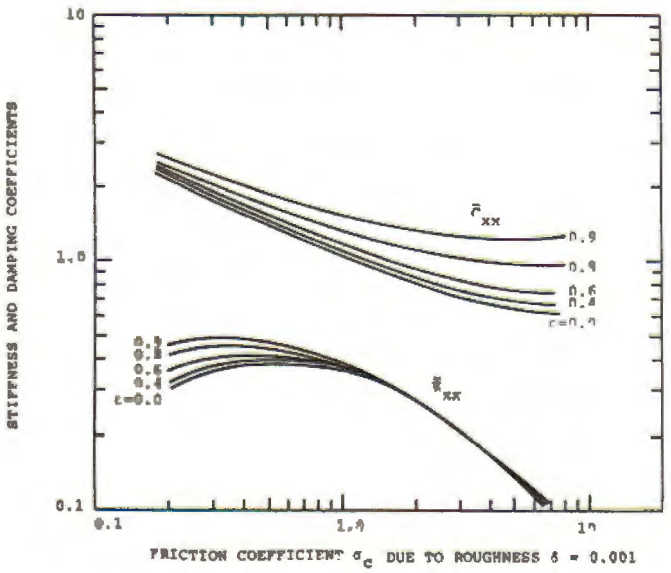

Fig. 6 Stiffness $\bar{K}_{xx}$ and damping $\bar{C}_{xx}$ vs friction due to roughness at different eccentricity ratios.

As noted in the "Introduction," the original rotor design included labyrinth seals and soft bearing supports to keep the first two critical speeds below the lowest operating speed of 23,000 rpm. In tests, the pump was found to have large subsynchronous vibrations starting near 17,000 rpm and continuing up into the operating speed range. The labyrinth seals were calculated to have a stiffness in the range 3.51×10^6 through 7.02×10^6 N/m (20,000-40,000 lb/in.), and the bearing-support stiffness in the range 3.5×10^7-7.02×10^7 N/m (200,000-400,000 lb/in.). The labyrinth seals had negligible stiffness and low damping values as well. After replacing the labyrinth seals with the three land seals and stiffening the supports, the pump ran above 32,000 rpm with no large subsynchronous vibration.

It should be noted that the analysis of a centered seal includes the effect of shaft rotation.[4,5,7-9] This produces cross-coupled stiffness K_{xy} and K_{yx}, which tend to make the rotor less stable. As yet, no complete theory for eccentric seals exists to calculate these coefficients. Usually the centered values are used as a reasonable approximation.

Conclusions

1) A perturbation analysis has been carried out for eccentric plain seals with high axial flow rates. Load capacity, stiffness, and damping of the seals have been calculated for a wide range of axial Reynolds number.

2) Load capacity curves peak for some value of axial Reynolds number. At low Reynolds number, the pressure drop around the seal is primarily due to friction loss, and only small pressure gradients are generated around the seal. At higher values of Reynolds numbers, the Bernoulli effect becomes stronger, and load capacity increases due to higher pressure gradients around the seal. At very high axial Reynolds number, large head losses occur at the entrance to the seal so that the pressure tends toward a constant value around the shaft. Thus the load capacity again becomes small.

3) A correction factor for the seal length-to-radius ratio has been included in the analysis. This correction factor was originally developed by Black and Jensen[4] for seals with a longer L/D ratio. Although no direct verification of this correction factor for longer seals at high Reynolds numbers is

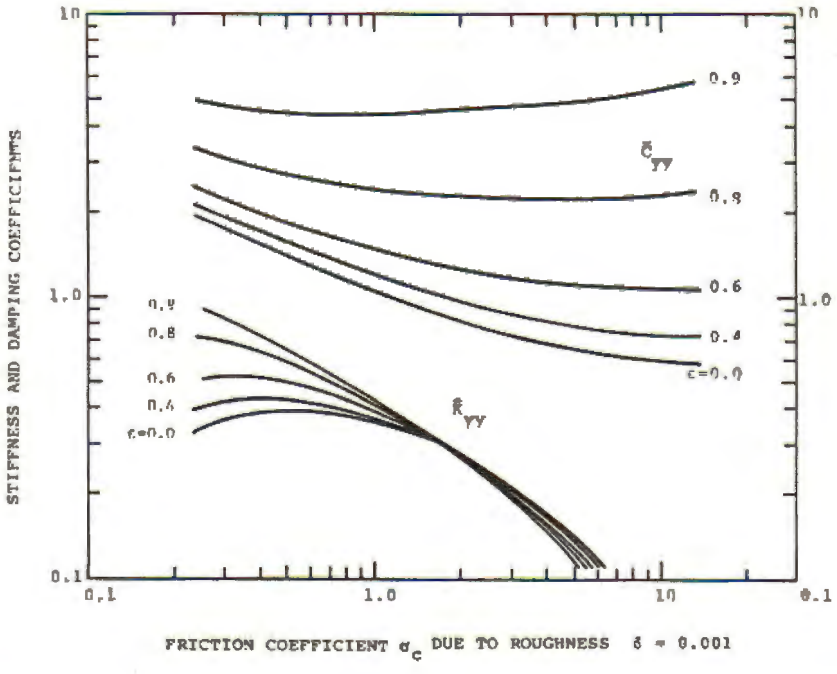

Fig. 7 Stiffness $\bar{K}_{yy}$ and damping $\bar{C}_{yy}$ vs friction due to roughness at different ratios.

available, it is felt that this is probably better than not taking into account the correction factor (see Appendix C).

4) Design parameters for a three-stepped plain seal were calculated for the Space Shuttle main engine hydrogen turbopump. The calculations indicated that the stiffness and damping of these recommended seals would be much higher than the existing labyrinth-type seals. A full-scale dynamic analysis of the hydrogen turbopump indicated that stiffening the seals would increase the stability threshold of the turbopump by about 6000 or 7000 rpm. When installed and operated, these seals plus stiffening of the bearing support structure did produce a very substantial increase in stability from approximately 17,000 up to 32,000 rpm.

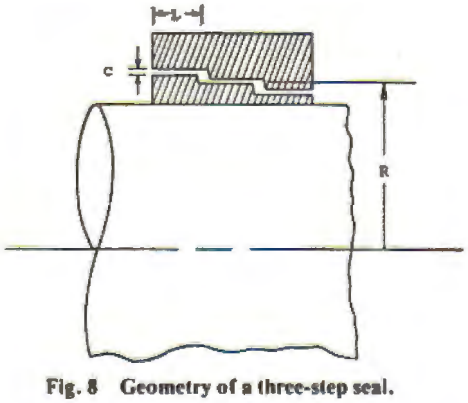

Fig. 8 Geometry of a three-step seal.

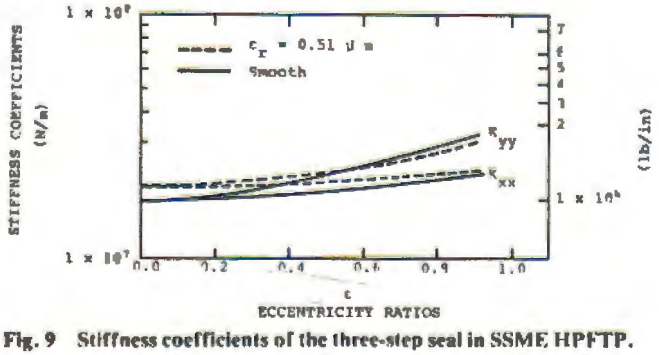

Fig. 9 Stiffness coefficients of the three-step seal in SSME HPFTP.

5) The analysis of short plain fields at axial Reynolds numbers has been extended to include surface roughness by inclusion of a rough pipe formula due to Colbrook.[16]

Appendix A: Friction Factor

The friction coefficients of the pressure-induced flow across annulus seals have been investigated theoretically by Tao and Donovan.[14] Yamada[11] experimentally measured the friction factor for the axial Reynolds number up to 10^4 and gave the formula $\lambda = 24/Re$ for laminar flow and $\lambda = 0.079\,Re^{-\frac{1}{4}}$ for turbulent flow.

The friction becomes roughness-dependent with high axial Reynolds number.[15] Correlation of the friction coefficient due to roughness is based on the rough pipe formula by Colebrook[16]:

$$4\lambda = a + bRe^{-c}$$

$$a = 0.094\delta^{0.225} + 0.53\delta$$

$$b = 88\delta^{0.44}$$

$$c = 1.62\delta^{0.134}$$

where δ is relative roughness.

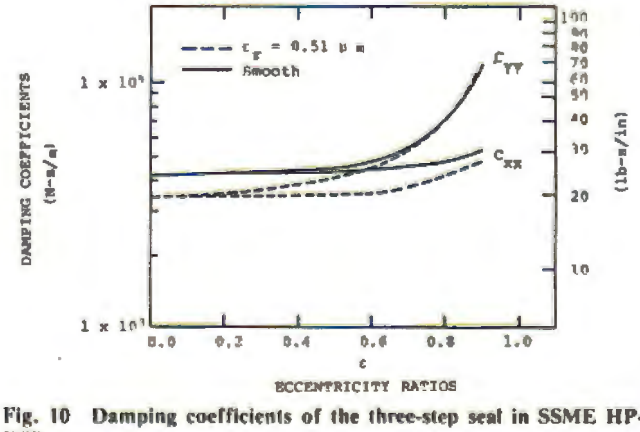

Fig. 10 Damping coefficients of the three-step seal in SSME HP-FTP.

Appendix B: Local Fluid Acceleration

The purpose of this Appendix is to examine the effect of the local fluid acceleration term $\partial u/\partial t$ in the momentum Eq. (2):

$$-\frac{1}{\rho}\frac{\partial p}{\partial z}=\lambda\frac{u^2}{h}+u\frac{\partial u}{\partial z}+\frac{\partial u}{\partial t}$$

Black and Jenssen[4] developed an analysis for centered seals including shaft rotation. The forces were obtained as

$$\begin{Bmatrix}F_x\\F_y\end{Bmatrix}=-\frac{\pi R\Delta p}{\lambda}\left\{\begin{bmatrix}\mu_0-\frac{1}{4}\mu_2\omega^2T^2 & \frac{1}{2}\mu_1\omega T\\ -\frac{1}{2}\mu_1\omega T & \mu_0-\frac{1}{4}\mu_2\omega^2T^2\end{bmatrix}\begin{Bmatrix}X\\Y\end{Bmatrix}+\begin{bmatrix}\mu_1T & \mu_2\omega T^2\\ -\mu_2\omega T^2 & \mu_1T\end{bmatrix}\begin{Bmatrix}\dot X\\ \dot Y\end{Bmatrix}+\begin{bmatrix}\mu_2T^2 & 0\\0 & \mu_2T^2\end{bmatrix}\begin{Bmatrix}\ddot X\\ \ddot Y\end{Bmatrix}\right\}$$

For zero shaft rotation, this reduces to

$$\begin{Bmatrix}F_x\\F_y\end{Bmatrix}=-\frac{\pi R\Delta p}{\lambda}\left\{\begin{bmatrix}\mu_0 & 0\\0 & \mu_0\end{bmatrix}\begin{Bmatrix}X\\Y\end{Bmatrix}+\begin{bmatrix}\mu_1T & 0\\0 & \mu_1T\end{bmatrix}\begin{Bmatrix}\dot X\\ \dot Y\end{Bmatrix}+\begin{bmatrix}\mu_2T^2 & 0\\0 & \mu_2T^2\end{bmatrix}\begin{Bmatrix}\ddot X\\ \ddot Y\end{Bmatrix}\right\}$$

Neglecting the local acceleration $\partial u/\partial t$ is equivalent to neglecting μ_2T^2.

For σ_c in the range of 0.55, the μ_2 values are about[4]

$$\mu_0\cong 0.05 \qquad \mu_1\cong 0.2 \qquad \mu_2\cong 0.035$$

Considering the SSME seal from the section on "Stiffness and Damping Coefficients," the mean flow time T is approximately 4.35×10^{-5} s for an axial Reynolds number of 524,200. This gives an effective acceleration term of approximately 6.6×10^{-11} s^{-2}, whereas the velocity term is 8.7×10^{-6} s^{-1}. Even assuming a sinusoidal shaft oscillation at operating speed of 3.5×10^3 rad/s, the acceleration term times the speed is only 2.3×10^{-7} s^{-1}. Thus the acceleration terms are neglected.

The very small mean passage time is due to the very low viscosity of liquid hydrogen. It appears very reasonable to neglect the local acceleration term in this case. The authors have not investigated the effect that $\partial u/\partial t$ has on a lower Reynolds number. However, Jenssen[17] notes good agreement between nonlinear seal calculations and experimental results for a water seal in the range $Re=10{,}000$. The local acceleration term was neglected in the calculations.

Appendix C: L/R Effect

This analysis has assumed that the seal length is small compared to the diameter. Black and Jenssen[4] have developed modification factors α and β for μ_0 and μ_1, respectively, when the finite length of the seal was taken into account:

$$\alpha=\frac{1}{1+0.28(L/R)^2} \qquad \mu_0=\alpha\mu_0$$

$$\beta=\frac{1}{1+0.23(L/R)^2} \qquad \mu_1=\beta\mu_1$$

The factors were actually developed for the dynamic coefficients, but μ_0 here will also be used for load capacity calculation.

Acknowledgments

The authors would like to thank H. F. Black for his very helpful suggestions concerning this work. This study was supported in part by NASA Contract No. NAS8-31951-5 (administered by the Marshall Space Flight Center, Huntsville, Ala.) and Energy Research and Development Agency Contract No. EF-76-2479.

References

[1] Lomakin, A. A., "Calculation of Critical Speed and Securing of Dynamic stability of Hydraulic High-Pressure Pumps with Reference to the Forces Arising in the Gap Seals," *Energomashinostroenie*, Vol. 4, No. 1, 1958, p. 1158.

[2] Marcinkowskij, W. A. and Karincey, J. B., "Influence of Gap Seals on the Critical Speeds of Feed Pump Rotors," *Energomashinostroenie*, Vol. 7, No. 4, 1961.

[3] Black, H. F., "Effects of Hydraulic Forces in Annular Pressure Seals on the Vibrations of Centrifugal Pump Rotors," *Journal of Mechanical Engineering Science*, Vol. 11, Feb. 1969, pp. 206-213.

[4] Black, H. F. and Jenssen, D. N., "Dynamic Hybrid Bearing Characteristics of Annular-Controlled Leakage Seals," *Institute of Mechanical Engineers*, Vol. 184, Pt. 3N, Sept. 1970, pp. 92-100.

[5] Black, H. F. and Murray, J. L., "The Hydrostatic and Hybrid Bearing Properties of Annular Pressure Seals in Centrifugal Pumps," BHRA RR1026, 1969.

[6] Black, H. F., "On Journal Bearings With High Axial Flows in the Turbulent Regime," *Journal of Mechanical Engineering Science*, Vol. 12, April 1970, pp. 301-303.

[7] Black, H. F. and Jenssen, D. N., "Effects of High-Pressure Ring Seals on Pump-Rotor Vibrations," Fluids Engineering Div., American Society of Mechanical Engineers, Paper 71-WA/FE-38, 1971, pp. 1-5.

[8] Black, H. F. and Cochrane, E. A., "Leakage and Hybrid Bearing Properties of Serrated Seals in Centrifugal Pumps," Paper G5, *6th International Conference on Fluid Sealing*, Munich, 1973, pp. 61-70.

[9] Black, H. F., "Lateral Stability and Vibrations of High-Speed Centrifugal Pump Rotors," *Dynamics of Rotors Symposium Lyngby/Denmark*, edited by F. I. Niordson, Springer-Verlag, Berlin, 1975, pp. 57-74.

[10] Hirs, G. G., "A Bulk-Flow Theory for Turbulence in Lubricant Films," *Journal of Lubrication Technology*, Vol. 95, Ser. F., April 1973, pp. 137-146.

[11] Yamada, Y., "Resistance of a Flow Through an Annulus with an Inner Rotating Cylinder," *Bulletin of Japan Society of Mechanical Engineers*, Vol. 5, No. 18, May 1962, pp. 302-310.

[12] Yamada, Y., Nakabayashi, K., and Maeda, K., "Pressure Drop Measurements of the Flow-Through Eccentric Cylinders with Rotating Inner Cylinders," *Bulletin of Japan Society of Mechanical Engineers*, Vol. 12, No. 53, Dec. 1969, pp. 1032-1040.

[13] Kaye, J. and Elgar, E. C., "Modes of Adiabatic and Diabatic Fluid Flow in an Annulus With an Inner Rotating Cylinder," *Transactions of ASME*, Vol. 80, April 1958, pp. 753-765.

[14] Tao, L. N. and Donovan, W. F., "Through-Flow in Concentric and Eccentric Annuli of Fine Clearance With and Without Relative Motion of the Boundaries," *Transactions of ASME*, Vol. 77, Nov. 1955, pp. 1291-1301.

[15] Streeter, V. L. and Wylie, E. B., *Fluid Mechanics*, McGraw-Hill, New York, 1975.

[16] Colebrook, C. F., "Turbulent Flow in Pipes With Particular Reference to the Transition Region Between the Smooth and Rough Pipe Laws," *Journal of the Institute of Civil Engineering (London)*, Vol. 11, 1938-1939, pp. 133-156.

[17] Jenssen, D. N., "Dynamics of Rotor Systems Embodying High-Pressure Ring Seals," Ph.D. Thesis, Heriot-Watt Univ., Edinburgh, Scotland, 1970.